Magnetic cotton textile wastes pyrolyzed by ferric cerium oxide for degradation of p-nitrophenol by catalytic ozonation

Xiaojie Fu, Yuanxing Huang, Zhihao Jin, Liang Li and Zhiguo Zhang

ABSTRACT

In this paper, magnetic cotton textile wastes pyrolyzed by ferric cerium oxide (Fe_xCe_y oxide/PC) were synthesized for degradation of p-nitrophenol by catalytic ozonation, and the optimal Fe-Ce ratio was 10:1. Compared to $Fe_{10}Ce_1$ oxide, the $Fe_{10}Ce_1$ oxide/PC not only greatly improved the degradation efficiency of PNP, but also reduced the dosage of catalyst. Through the BET test, the $Fe_{10}Ce_1$ oxide/PC has a high specific surface area to absorb part of the pollutants. VSM test shows that the material is magnetic and easy to recycle. Response surface methodology (RSM) was applied to optimize the experimental condition, and the optimal removal rate was 90% when the initial pH was 9, the catalyst dosage was 0.4 g/L, and the ozone addition was 1.77 L/min (5.9 mg/L). Finally, the mechanism of PNP degradation was explored utilizing inhibitor and ESR free radical detection. The adsorption capacity of the material and electron-absorbing property of PNP jointly determined the high catalytic efficiency with $Fe_{10}Ce_1$ oxide/PC in catalytic ozonation.

Key words | catalytic ozonation, cotton textile wastes, p-nitrophenol, RSM

Xiaojie Fu
Yuanxing Huang (corresponding author)
Zhihao Jin
Liang Li
Zhiguo Zhang
School of Environment and Architecture,
University of Shanghai for Science and Technology,
Shanghai, 200093,
China
E-mail: *huangyuanxing@usst.edu.cn*

HIGHLIGHTS

- The optimum proportion of cotton textile waste pyrolysis was determined by oxide screening.
- The specific surface area of the oxide pyrolysis cotton textile wastes is larger than that of the oxide itself and it is magnetic to recycle.
- Inhibitors and free radical detection proved that catalytic ozonation follows hydroxyl radical mechanism.
- The response surface method was used to explore the optimal process parameters.

INTRODUCTION

Phenolic compounds are the main pollutants in many industrial wastewaters, which often bring a series of problems because of their high toxicity and persistence (Canizares *et al.* 2005). P-nitrophenol (PNP) has been widely used as an intermediate in pesticides, medicine, explosives, dye-wood preservatives, etc. Acute exposure to PNP could lead to anemia, eye and skin irritation, liver damage or systemic poisoning (Chen *et al.* 2018). PNP has been listed as a priority pollutant and the US environment agency limited its level in water to less than 10 ng/L (Chen *et al.* 2016). Because of its toxicity to many organisms, it is often difficult to biodegrade when discharged into industrial wastewater (Pang & Lei 2016). In recent years, advanced oxidation technologies such as photocatalysis, Fenton and electrochemical oxidation have been frequently

doi: 10.2166/wst.2021.131

used in the treatment of PNP wastewater (Yu *et al.* 2010; Zhang *et al.* 2016; Pang & Lei 2016; Chen *et al.* 2018; Rodrigues *et al.* 2018), and especially catalytic ozonation is more and more widely used due to the advantage of green and high efficiency (Yuan *et al.* 2018; Li *et al.* 2021).

Ozone is widely used in air disinfection and water treatment as an effective oxidant (Wang & Bai 2017; Zhang *et al.* 2020). Ozone oxidation is carried out in two ways: (a) direct oxidation by ozone molecules; (b) ozone decomposition generates hydroxyl radicals for indirect oxidation (Yuan *et al.* 2018; Wang & Chen 2020). The direct oxidation of ozone is selective and cannot completely degrade pollutants into carbon dioxide and water. The ozone molecule has an electrophilic center and a nucleophilic center, which could bind H(electrophilic) and O(nucleophilic) atoms of the surface hydroxyl groups, then the bridging could be converted to hydroxyl radicals through electron transfer. Therefore, catalytic ozonation technology, especially heterogeneous catalytic ozonation technology, has been increasingly studied.

In recent years, catalytic ozonation by transition metal oxides, especially iron oxides, has been extensively studied. Zhao *et al.* (2013) studied the effect of magnetic substance $NiFe_2O_4$ on catalytic ozonation for the removal of phenolic pollutants, and the metal oxides showed a high effect in the catalytic ozonation. Shahzad Afzal *et al.* studied the different efficiency of catalytic ozonation degradation of PNP due to different electron transfer of cerium dioxide exposed to a crystal face. Cerium oxide is widely used in oxygen sensors, thermal coal combustion and other fields due to its rich oxygen vacancy and multi-acid and base properties. Electron transfer between Ce^{3+}/Ce^{4+} plays an important role in catalytic ozone efficient degradation of pollutants (Afzal *et al.* 2019). The catalytic mechanism was often associated with double metal materials charge transfer (Yuan *et al.* 2018; Fang *et al.* 2019). Dai *et al.* (2014) loaded CeO_2 on activated carbon as the catalyst in ozonation to remove p – TSA. Compared with single activated carbon, the metal oxide-supported activated carbon not only reduced the catalyst dosage, but also improved the removal effect by nearly 2 times. However, due to the non-renewable nature of activated carbon and the challenges of the catalyst's recycling, the searing of green catalyst is a new topic.

Cotton textile wastes have high yield but improper treatment (Ohmukai *et al.* 2008). The mechanical treatment of cotton textile wastes required great technical level and caused environmental pollution. Therefore, it is of significance to explore green methods to treat cotton textile wastes. Xu *et al.* (Qi *et al.* 2020) studied the activation of magnetic activated carbon impregnating with $FeCl_3$, which took cotton textile wastes as raw materials. Cotton textile wastes modified by $FeCl_2$, $FeCl_3$, and $ZnCl_2$ had a great advantage in adsorbing pollutants (Xu *et al.* 2018; Tian *et al.* 2019). Shou Li *et al.* synthesized $CoFe_2O_4$ @ biochar for catalytic ozonation degradation of bisphenol A, and the pollutant removal rate reached 95.85%. Compared with bimetallic oxides, the addition of biochar made the catalyst have the advantages of smaller pore size and smaller volume, so it achieved better pollutant removal effect (Li *et al.* 2021). The pyrolysis of cotton textile wastes with bimetallic oxides is environmentally friendly and its application in catalytic ozonation for removal of organic matter is rarely reported.

The traditional experimental design adopts single-factor experiments, which involve many experimental groups, but the interaction between different experimental factors is not considered, thus it would be hard to apply in large-scale experiments (Shen *et al.* 2017; Asgari *et al.* 2020). Box-Behnken experiments of response surface methodology (RSM) could fit functions in variables, evaluate the relationship between experimental conditions and response values through a series of parameters of the regression equation, and then analyze the interaction of experimental factors in a limited number of experimental groups to estimate the best experimental conditions (Wu *et al.* 2017; Malakootian *et al.* 2020).

In this paper, the magnetic cotton textile wastes were pyrolyzed with ferric cerium oxide, and the synthesized material was used as catalyst to degrade p-nitrophenol in water by catalytic ozonation. Through a series of characterizations, the mechanism of catalytic ozonation was explored. In the end, the RSM experiment was designed to explore the influence of different experimental conditions on the removal rate of PNP by catalytic ozonation.

MATERIALS AND METHODS

Source of materials

Cotton textile wastes from the first cotton mill in Wuxi, Jiangsu province, were used as the main raw materials for the pyrolysis of activated carbon. The drugs used in this experiment were all at the analytical level. P-nitrophenol (PNP) was purchased from national medicine (purity >99%). Other chemical reagents were purchased from Alighting Reagent Net (Shanghai). In the experiment, both

NaOH and HCl used to adjust the initial pH were configured with deionized water.

Preparation process of catalyst

The composite oxide was prepared by the hydrothermal method. A certain amount of Ce $(Cl)_3 \cdot 6H_2O$ and $Fe(Cl)_3 \cdot 9H_2O$ were dissolved in deionized water and stirred evenly to obtain metal salt solutions with different molar ratios. Then the prepared solution was placed on a magnetic stirrer and 5 mol/L of ammonia water was slowly added to keep the pH at 10. After stabilization, the 60 mL mixed solution was transferred to a 100 mL stainless steel reactor, which reacted for 48 h at 180 °C. After cooling, the sample was washed several times to neutral with distilled water, and the precursor of composite oxide was dried in the oven. Finally, the material was calcined at 500 °C for 10 h to get the required red Fe_XCe_y oxide.

The catalyst used the impregnation method to pyrolyze cotton textile wastes. $Ce(Cl)_3 \cdot 6H_2O$ and $Fe(Cl)_3 \cdot 9H_2O$ were prepared as salt solutions, then 5 g cotton textile wastes were cut at about 0.5 cm and soaked in a beaker for 24 h before being taken out and dried in an oven at 60 °C for 24 h. Then, the sample-loaded quartz boat was placed in a tube furnace, which was blown off for about 20 minutes under the protection of N_2 with a flow rate of 100 cm^3/min. Finally, it was heated to 500 °C at 10 °C/min in the tube furnace and pyrolyzed for 60 minutes at 500 °C. When the tube furnace temperature dropped to room temperature, the roasted material was taken out and rinsed with ionized water until neutral. After drying in the oven at 80 °C, the material was Fe_XCe_y oxide/PC.

Apparatus and experimentation

The ozone gas used in the study came from an ozone generator (KX – S10, Kangxiao Environment Production Equipment Shanghai). The calcined oxide used a muffle furnace (SX2-4-13N, Shanghai Yiheng Scientific Instrument). Total organic carbon (TOC) was detected by (Multi N/C 3100, Jean, Germany). A vacuum drying oven was used for drying (Model DZF-6020, Shanghai Yiheng Science Instrument).

The p-nitrophenol solution, with an initial concentration of 20 mg/L, was prepared at room temperature. A certain amount of catalyst was weighed and added to the pollutant solution. Then ozone gas was pumped in. To fully disperse ozone gas in the water, the ozone gas flow rate could be accurately controlled by the mass flowmeter. Ozone concentration in solution could be detected by the indigo method and sampled at fixed time intervals (Bader & Hoigné 2013). After it was pumped into an inert gas, the sample was filtrated through a 0.45 μm membrane to remove the solid catalyst. Then the TOC of the sample was detected by a TOC analyzer. All experiments were repeated three times, and the final data was gotten after the three experiments.

Characterization methods

X-ray diffraction spectroscopy (XRD, Bruker D8 Advance, Karlsruhe, Germany) was used to detect the crystal structure at Cu-K_α (40 kV, 40 mA). The Brunauer-Emmett-Teller (BET) surface areas, total pore volume, and average pore size of the catalyst were measured by nitrogen adsorption and desorption under 77 K condition (ASAP 2020, Micromeritics, USA). The chemical morphology and molecular structure of the materials were analyzed using X-ray photoelectron spectroscopy (XPS, ESCALAB 250XL, USA) and scanning electron microscopy (SEM, S4800, Hitachi, Japan). X-ray energy spectrum analysis (EDS) mapping detection was used to detect the distribution of metal elements. Electron spin resonance (ESR, Brock A300) was used to detect hydroxyl radicals. A vibrating sample magnetometer (VSM) detected the magnetic properties of materials.

Response surface methodology

Response surface design describes the relationship between response value Y and variable X_i, which is used to describe the effect of experimental variables and the relationship between variables (Li *et al.* 2020). Applying the Box-Behnken of Design-Expert 8.0.6 software took response surface design (Derakhshan & Fazeli 2018). Firstly, the response value was the TOC removal rate of the PNP, and the variables were the dosage of catalyst, pH value of the initial solution and the addition of ozone. The range of the three variables was locked to the high, middle and low values after pre-experiment, which were represented by −1, 0, 1, and their code as shown in Table 1. According to the number of

Table 1 | Code of different experiment conditions

Actors / Code	Level −1	0	+1
pH	5	7	9
The dosage of catalyst (g/L)	0.1	0.25	0.4
The addition of ozone (L/min)	0.2	1.0	1.8

experimental groups designed by the software, the experimental results were filled into Table 2 after the experiment. At this time, the software would establish a multivariate quadratic function relationship between experimental variables and response values (Wang *et al.* 2019):

$$Y = b_0 + \sum b_i X_i + \sum b_{ii} X_i^2 + \sum b_{ij} X_i X_j + \varepsilon \quad (1)$$

Y represents the response value, namely the TOC removal rate of PNP. The b_0 is a constant; X_i is the variable; b_i represents the linear coefficient of the corresponding X_i; b_{ij} is the interaction coefficient; b_{ii} represents the second-order effect of the regression coefficient; ϵ refers to the statistical error and the interference caused by uncontrollable noise factors (Asgari *et al.* 2020).

At this time, the accuracy of the established function model could be verified by ANOVA, diagnostic analysis, and graph analysis. If these requirements cannot be met, the response surface model will not be obtained. Otherwise, the function model could be re-established (Shen *et al.* 2017).

Table 2 | Encode the corresponding experimental results

Run	Factor 1 A:the addition of ozone L/min	Factor 2 B:pH	Factor 3 C:the dosage of catalyst g/L	Response 1 The removal rate %
1	0	0	0	63.5
2	1	0	−1	82.7
3	1	0	1	92.3
4	−1	0	−1	26.5
5	−1	−1	0	34.7
6	1	1	0	77.1
7	0	0	0	65.3
8	0	0	0	63.7
9	−1	0	1	44.4
10	0	0	0	65.2
11	0	−1	−1	69.8
12	0	0	0	64
13	0	−1	1	76
14	1	−1	0	68.7
15	0	1	1	78.6
16	0	1	−1	70.3
17	−1	1	0	36.9

CONSEQUENCE AND RESULTS

The superiority of $Fe_{10}Ce_1$ oxide/PC

Ferric cerium oxides of different metal proportions were prepared by hydrothermal method then the catalytic effect was evaluated by catalytic ozonation in the degradation of PNP. As shown in Figure 1(a), when the initial TOC content was 10.5 mg/L, the ozone flux was 6.2 mg/L, and the oxide dosage was 1.0 g/L, the TOC degradation efficiency was compared after adding different catalysts for 60 min. The TOC content in the histogram decreased from the initial 10.5 mg/L to less than 2 mg/L and the point diagram shows the best TOC removal rate when the cerium iron ratio was 10:1. Therefore, the $Fe_{10}Ce_1$ oxide with the optimal catalytic ozonation efficiency was used as the precursor for pyrolysis of cotton textile wastes. Figure 1(b) shows the degradation efficiency of PNP in a system of solo ozone, $Fe_{10}Ce_1$ oxide or $Fe_{10}Ce_1$ oxide/PC catalytic ozone, and single adsorption respectively. Similarly, the histogram represents the proportion of TOC content at the sampling point to the initial TOC, and the point diagram represents the removal efficiency of TOC. The initial PNP concentration and ozone dosage remain unchanged, but the catalyst dosage was reduced to 0.4 g/L. After 25 min of catalytic ozonation, the TOC removal efficiency of $Fe_{10}Ce_1$ oxide/PC reached 90%, while the $Fe_{10}Ce_1$ oxide only reached 70%. When O_3 gas was not added, PNP degradation could be achieved by the adsorption of $Fe_{10}Ce_1$ oxide/PC but $Fe_{10}Ce_1$ oxide could not be. Therefore, the advantage of $Fe_{10}Ce_1$ oxide/PC was not only an additive amount by 0.25 times of the $Fe_{10}Ce_1$ oxide, but also the reaction time could be shortened to 25 min, which greatly improved the TOC degradation efficiency. The first-order kinetics (Figure 1(c) and 1(d)) could well represent the reaction efficiency of PNP degradation in different reaction systems when other conditions remain unchanged. To explore the properties of materials, a series of characterization was carried out.

Characteration

Figure 2(a) shows the XRD test diagram of the two catalysts. The $Fe_{10}Ce_1$ oxide test diagram was following the characteristic peaks of Fe_2O_3 (JCPDS No.33-0664) and CeO_2 (JCPDS No.34-0394), which indicates that the synthesized oxide is mainly composed of these two substances (Lv *et al.* 2010). The characteristic peaks of $Fe_{10}Ce_1$ oxide/PC were slightly

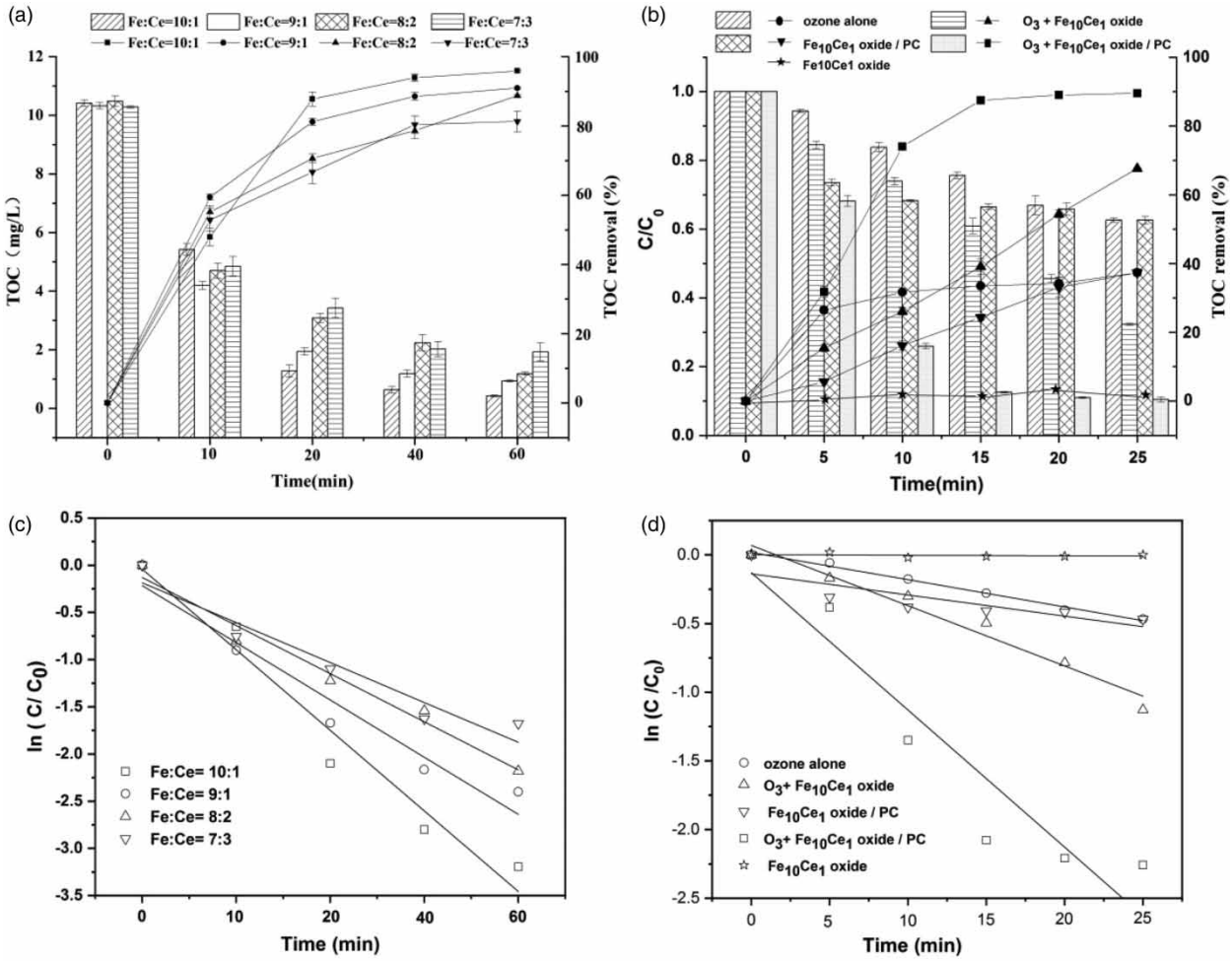

Figure 1 | (a) Different Fe-Ce ratio oxides degraded PNP in catalytic ozonation; (b) contrast between different systems in the degradation of PNP; (c) the first-order kinetics fitting under different Fe-Ce ratio oxides; (d) the first-order kinetics fitting under different systems.

shifted, but it was consistent with the characteristic peaks of Fe_3O_4 (JCPDS No.19-0609), and the characteristic peaks of CeO_2 also existed. After the introduction of carbon material, the types of metal oxides also changed, which may be related to the fiber of the carbon material, so the valence of iron in the material changed, but the cerium oxide did not change (Lv *et al.* 2012).

Figure 2(b) shows the nitrogen adsorption-desorption isotherms of BET. The isotherms of both catalysts contained mesoporous hysteretic rings, and no apparent saturated adsorption platform indicated that the pore structure of the two materials was not orderly (Zhang *et al.* 2016). The $Fe_{10}Ce_1$ oxide has a typical H3 hysteretic loop adsorption isotherm (Qi *et al.* 2017). The holes were mainly narrow slots formed by the accumulation of sheet particles and did not show adsorption saturation in the high relative pressure area. The $Fe_{10}Ce_1$ oxide/PC belongs to the H4 hysteresis loop adsorption isotherm, and the material contains a narrow crack hole (Qi *et al.* 2017). The mesoporous distribution diagram is shown in the illustration in Figure 2(b). The main pore diameter of the $Fe_{10}Ce_1$ oxide/PC was distributed at 5 nm. And it also be seen from Table 3 that the average pore of $Fe_{10}Ce_1$ oxide/PC diameter is smaller. BET test shows that the specific surface area of $Fe_{10}Ce_1$ oxide/PC is about three times of $Fe_{10}Ce_1$ oxide, which also explains it has a better TOC removal rate in the adsorption experiment.

Figure 2(c) shows the hysteresis cycle curves of the two catalysts. $Fe_{10}Ce_1$ oxide/PC has nonlinear and reversible behaviors in the weak hysteresis cycle curve. In the right corner, the illustration is a local magnification of $Fe_{10}Ce_1$ oxide/PC, indicating that it has a good magnetic recyclability, while the $Fe_{10}Ce_1$ oxide is not magnetic. It could be seen

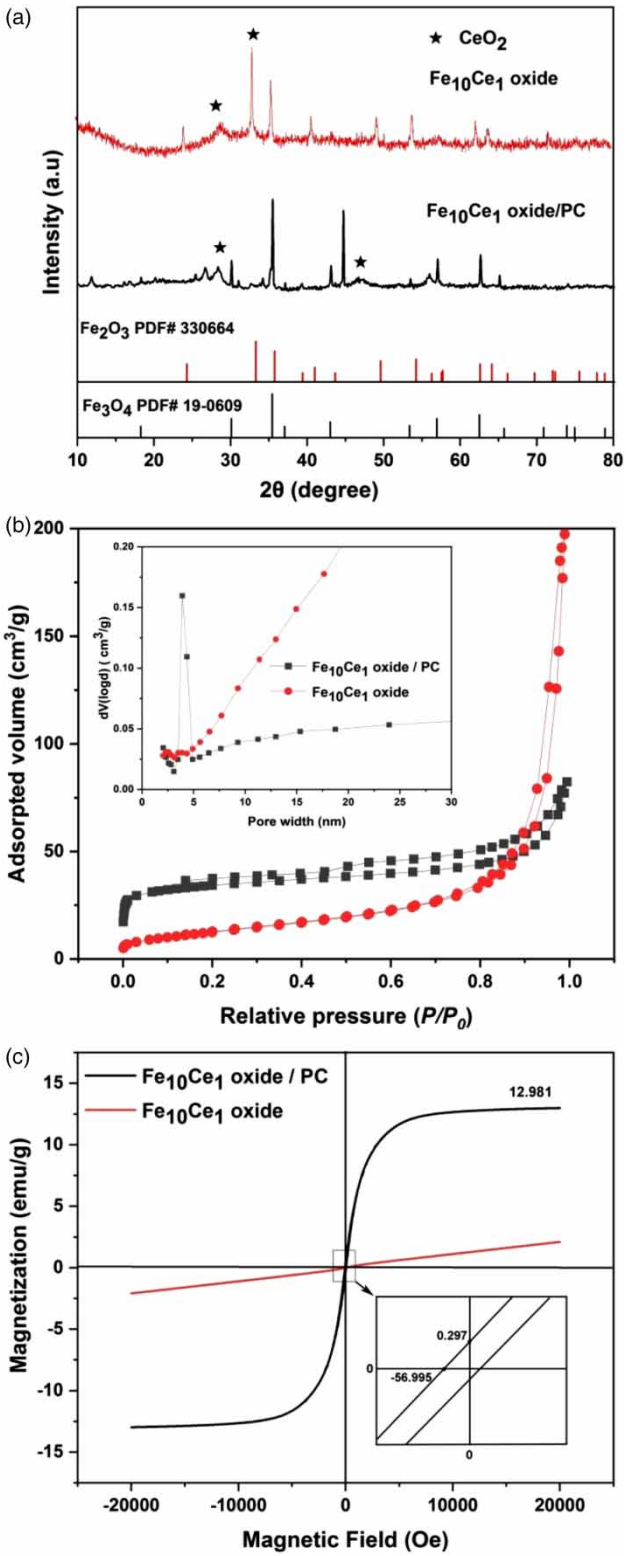

Figure 2 | (a) XRD patterns; (b) N_2 adsorption-desorption isotherms and (inset) BJH pore size distributions; (c) magnetization curves.

Table 3 | Surface area and pore volume

	S_{BET} ($m^2\ g^{-1}$)	Total pore volume ($cm^3\ g^{-1}$)	Average pore diameter (nm)
$Fe_{10}Ce_1$ oxide	46.917	0.319	20.269
$Fe_{10}Ce_1$ oxide/PC	121.974	0.088	9.282

that the saturated magnetization Hm of the $Fe_{10}Ce_1$ oxide/PC is 12.981 emu/g, the remanence intensity Br is 0.291 emu/g, and the correction tenacity degree Hc is 56.995 Oe, indicating high magnetic separation performance. Br/Hm is less than 0.03, which indicates that the $Fe_{10}Ce_1$ oxide/PC is superparamagnetic at room temperature and easy to magnetize or demagnetize (Qi *et al.* 2020). Therefore, the $Fe_{10}Ce_1$ oxide/PC has a better recovery rate to achieve solid-liquid separation.

Figure 3 is the SEM and EDS-Mapping detection diagram of $Fe_{10}Ce_1$ oxide/PC. The pyrolytic cotton textile wastes under transmission microscope with floc pattern and surface roughness, which may be the surface morphology formed by the adhesion of carbon fiber and oxide, make the catalyst have good porosity and high specific surface area to achieve the goal of adsorption and degradation of PNP. Based on the element scanning by EDS-mapping, it could be seen that Fe, Ce and O elements were evenly distributed in the material, and the element content detection also indicates that metal elements could be well introduced into the process of pyrolysis cotton textile wastes. The rich porosity of the material could absorb more PNP, and then the metal ions were evenly distributed on the surface of the catalyst could realize electron transfer in the process of catalytic ozonation; finally, it generated hydroxyl radicals with high oxidation to achieve the goal of rapid and thorough degradation of pollutants. Figure 4 is the XPS element detection atlas of the $Fe_{10}Ce_1$ oxide/PC. Figure 4(a) is a full scan of the elements of the material. It can be seen that there are four elements, Fe, Ce, C and O. Three distinct peaks could be observed in the O1s spectrum, where the peak of 529.4 eV is usually related to a bond of metal oxide, the peak of 532.4 eV represents the material surface association of water and water-adsorbed hydroxides, and the peak of 530.9 eV is usually related to the oxygen vacancy of metal oxide (Huang *et al.* 2016). This may be caused by the high-temperature pyrolysis of cotton textile wastes. A large number of studies have shown that the oxygen vacancy of metal oxides could

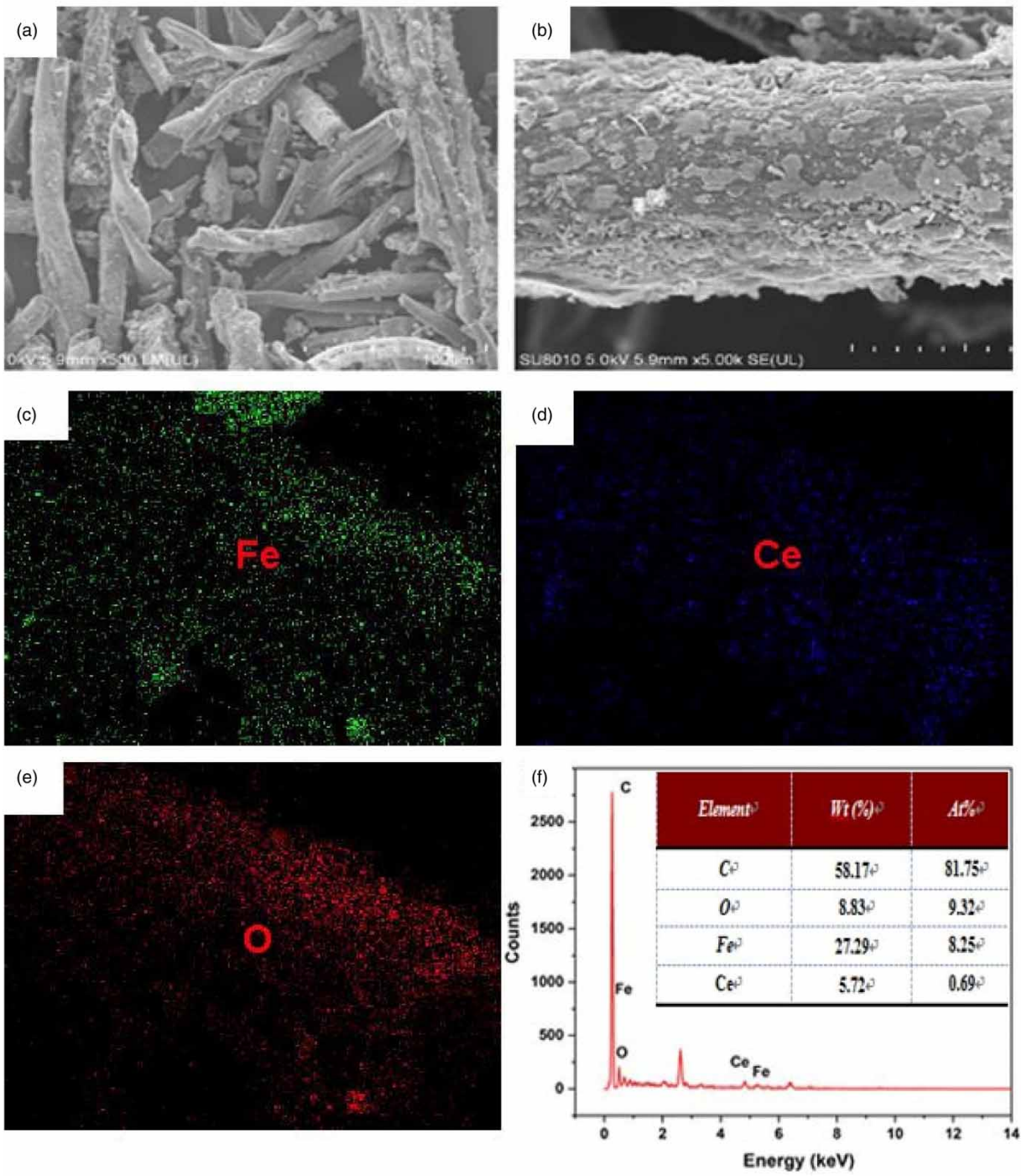

Figure 3 | SEM and EDS-mapping of $Fe_{10}Ce_1$ oxide/PC.

improve electron transfer efficiency and increase charge transfer (Huang *et al.* 2016; Xiao *et al.* 2020). This property is likely to be closely related to the high efficiency of PNP degradation with $Fe_{10}Ce_1$ oxide/PC in catalytic ozonation. In the Fe2p peaks separation spectrum, 711.97 eV of Fe 2p3/2 and 724.57 eV of Fe 2p1/2 are characteristic peaks of Fe_3O_4, which was consistent with the XRD pattern (Xu *et al.* 2020). In the Ce 3d optoelectronic map, 900.9 eV and 883.1 eV of Ce 3d3/2 spin-orbit are characteristic peaks of Ce^{4+}, then 897.5 eV and 917.0 eV are

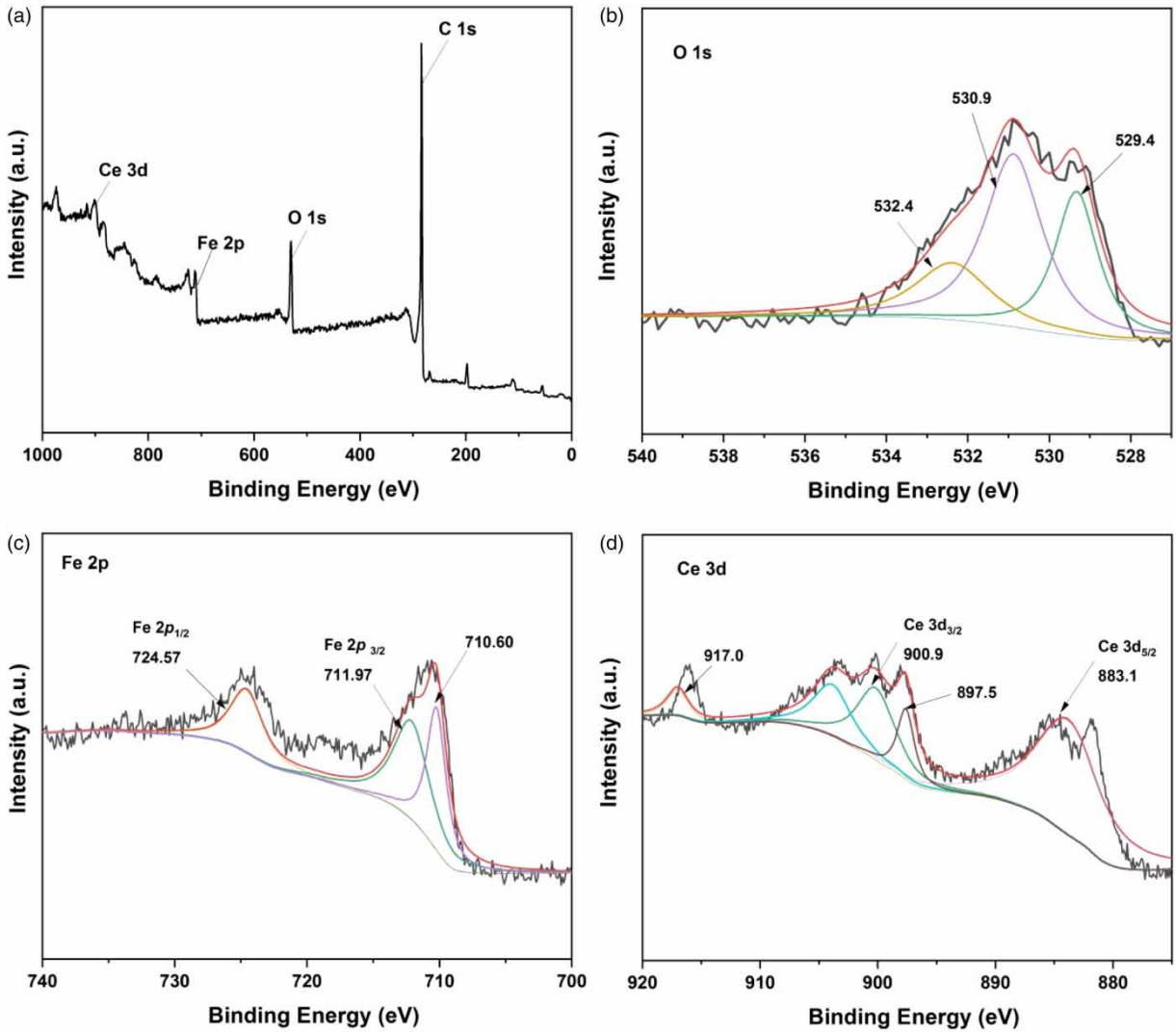

Figure 4 | (a) XPS survey spectra (b) O1s (c) Fe 2p (d) Ce 3d of $Fe_{10}Ce_1$ oxide/PC.

satellite companion peaks, which were in good accordance with CeO_2 detected in XRD (Huang *et al.* 2016).

RSM

Establishment of equation in RSM

In this study, the Box-Behnken experiment was designed by using Design-Expert 8.0.6 software. After the end of the experiment, the multivariate quadratic equation was established by the experimental results as follows:

$$Y = 46.32 + 60.07 * A - 4.42 * B - 142.85 * C + 0.97 * AB - 17.29 * AC + 1.75 * AC - 17.34 * A^2 + 0.28 * B^2 + 365.78 * C^2 \quad (2)$$

After ANOVA analysis of variance, as shown in Table S1 (supplementary document), the *P*-value is 0.0001 and the model is significant, which indicates the stability and significance of the model. At the same time, the F value of ozone dosage is the largest, indicating that this experimental condition has a significant influence on the experimental results (Wu *et al.* 2017). The regression coefficient R^2 is 0.972312, which indicates that the error of the regression equation is very small, and almost all the experimental sample points fall on the surface determined by the regression equation (Asgari *et al.* 2020). The normal distribution probability graph of the residual is shown in Figure S1. The predicted value and true value fitted into a straight line, indicating that the model is suitable to optimize the experimental conditions for the degradation of PNP with $Fe_{10}Ce_1$ oxide/PC in catalytic ozonation (Shen *et al.* 2017).

Interaction of the initial pH and dosage of ozone

Figure 5(a) and 5(b) show the response surface and contour diagram of the initial pH and dosage of ozone, respectively. In general, both the improvement of initial pH and the increase of ozone dosage could improve the removal efficiency of PNP, but the dosage of ozone has a greater impact on the response value. The response value changed little in the range of 5–9 of the initial pH value, which indicated that the catalyst had strong adaptability to pH when it degraded the PNP. The OH^- in the reaction solution is closely related to the formation of the surface hydroxyl groups occupying the Lewis acid position of the catalyst, while the electrophilicity and nucleophilicity of ozone could be connected with the H and O of the surface hydroxyl groups to produce •OH (Huang *et al.* 2019). The amount of Lewis acid position is limited, so excessive OH^- would generate competitive adsorption, then increasing pH value would slow down the rate of degradation of pollutants. Therefore, the optimal pH value could be found in the response surface.

Interaction of the addition of ozone and the dosage of catalyst

Figure 5(c) and 5(d) respectively show the catalyst dosing and ozone addition response surface and contour map. When catalyst dosage increased from 0.1 to 0.4 g/L, the pollutant removal rate is also enhanced, but when ozone addition increased, the pollutant removal rate increased even faster, which was also consistent with the results of ANOVA that F value was the maximum. The ozone addition increased fast in the range of 0.2–1.0 L/min, and slowed down significantly in the range of 1.0–1.8 L/min, indicating that the dissolution of ozone in water reached a saturated state. Therefore, the optimal ozone addition could be found on the surface.

Interaction of the dosage of catalyst and initial pH

Figure 5(e) and 5(f) respectively show the response surface and contour map of the catalyst dosage and the initial pH value of the solution. In general, the interaction between these two variables was not significant enough. When the initial pH remained unchanged and the catalyst dosage was 0.1–0.4 g/L, the pollutant removal efficiency response firstly decreased and then increased. The reason for this phenomenon was that the $Fe_{10}Ce_1$ oxide/PC itself could absorb pollutants to the surface for degradation. Under the condition of constant pollutant concentration, adding the amount of catalyst would lead to a competitive effect on the adsorption of pollutants so the addition of ozone would reduce the advantage of degradation brought by adsorption. Therefore, the optimal catalyst dosage could be found on the response surface.

Selection of optimal conditions

As shown in Table S2, the first set of data is the optimal condition selected by the software. However, based on

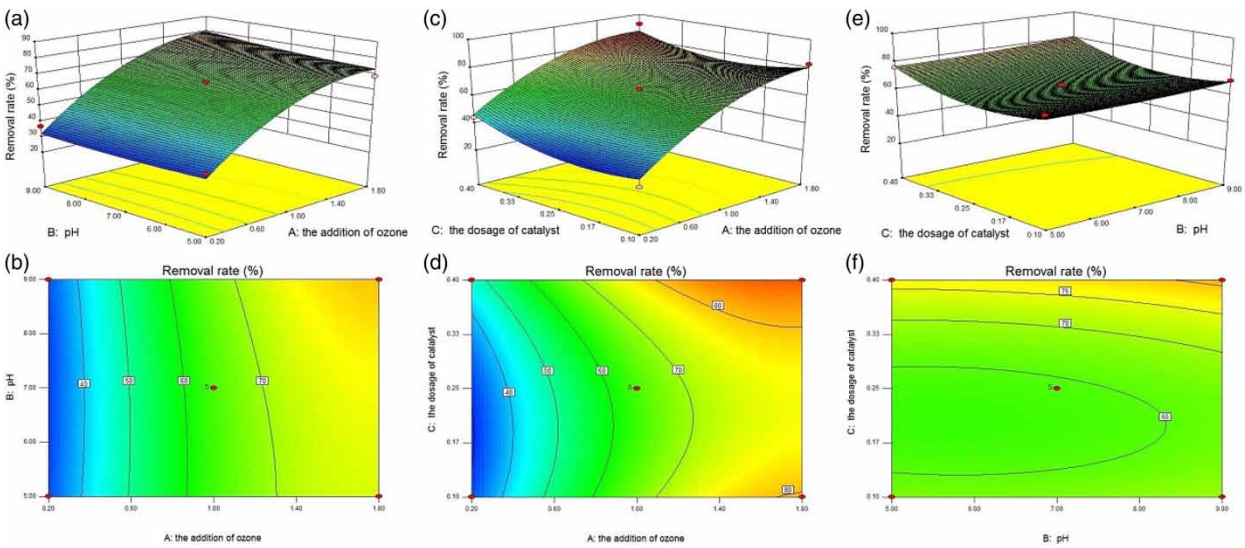

Figure 5 | Response surface diagram and contour maps of the effect of the initial pH, the dosage of catalyst and the concentration of ozone on the removal of PNP.

economic considerations, the optimal experimental conditions we selected were that the TOC removal rate was 91% when the initial pH of catalyst dosage was 9, the catalyst dosage was 0.4 g/L, and the ozone addition was 1.77 L/min (0.59 mg/L). After verification experiments, it was found that the difference in experimental results was within 5%. Therefore, the response surface could optimize the experimental conditions well.

Possible mechanism of degradation

Figure 6 shows the catalytic degradation mechanism of $Fe_{10}Ce_1$ oxide/PC. Figure 6(a) is the comparison diagram of TOC removal after adding HCO_3^- and PO_4^{2-} under the same experimental conditions. Studies have shown that HCO_3^- could quench OH^-, and PO_4^{2-} could occupy the active site of catalyst, so they could effectively reduce the removal efficiency of TOC, which also indirectly explains the mechanism of catalytic degradation of PNP (Huang *et al.* 2019). Figure 6(b) is the detection diagram of hydroxyl radical in the solution. In the single ozone system, no hydroxyl radical signal was detected, but in the $Fe_{10}Ce_1$ oxide/PC catalytic system, the hydroxyl radical signal was detected, which directly explains the mechanism of hydroxyl radical by catalytic ozonation.

According to the previous material characterization, the $Fe_{10}Ce_1$ oxide/PC was mainly composed of Fe_3O_4 and CeO_2 and the possible catalytic mechanism could be deduced. Firstly, ozone was connected to the surface of Fe_3O_4 ($FeOH^{2+}$) by electrostatic force or H bonding, which promoted electron conversion. -O and H-O were weakened into HO_2• and HO_3•. Then O_3 and HO_2• further reacted to form •OH to mineralize PNP. In order to complete the Redox pair and maintain the electrostatic charge balance, the lattice oxygen also reduced Fe^{3+} to Fe^{2+} and Ce^{4+} to Ce^{3+}. Therefore, the direction of electrons could be divided into three ways (Zhao *et al.* 2013; Shen *et al.* 2020): (1) ammonium group was generated due to the electron-absorbing properties of the PNP nitrate functional group; (2) generated Fe^{3+} and the original Fe^{3+} gained electrons to generate Fe^{2+}; (3) Ce^{4+} formed Ce^{3+}. There was competition between these approaches. Through the transfer of electrons between metal elements in the material, the formula is shown in (3)–(11) (Zhao *et al.* 2013; Afzal Quan & Lu 2019):

$$\equiv Fe^{2+} - OH_2^+ - 2O_3 \rightarrow \equiv Fe^{3+} + 2HO_3^{\bullet} + O^{2-} \quad (3)$$

$$HO_3^{\bullet} + HO_3^{\bullet} \rightarrow 2 \cdot OH + 2O_2 \quad (4)$$

$$2O^{2-} + H^+ \rightarrow HO \cdot_2^- \quad (5)$$

$$O_3 + HO_2^{\bullet} - \rightarrow \bullet OH + O_2^- + O_2 \quad (6)$$

$$NO_2^+ + O^{2-} + H_2O \rightarrow NH_2^- + 2O_2 \quad (7)$$

$$\equiv 4Fe^{3+} + 2O^{2-} \rightarrow \equiv 4Fe^{2+} + O_2 \quad (8)$$

$$\equiv 4Ce^{4+} + 2O^{2-} \rightarrow \equiv 4Ce^{3+} + O_2 \quad (9)$$

$$\equiv Ce^{3+} - OH_2^+ - 2O_3 \rightarrow \equiv Ce^{4+} + 2HO_3^{\bullet} + O^{2-} \quad (10)$$

$$O_2 + 4e \rightarrow 2O^{2-} \quad (11)$$

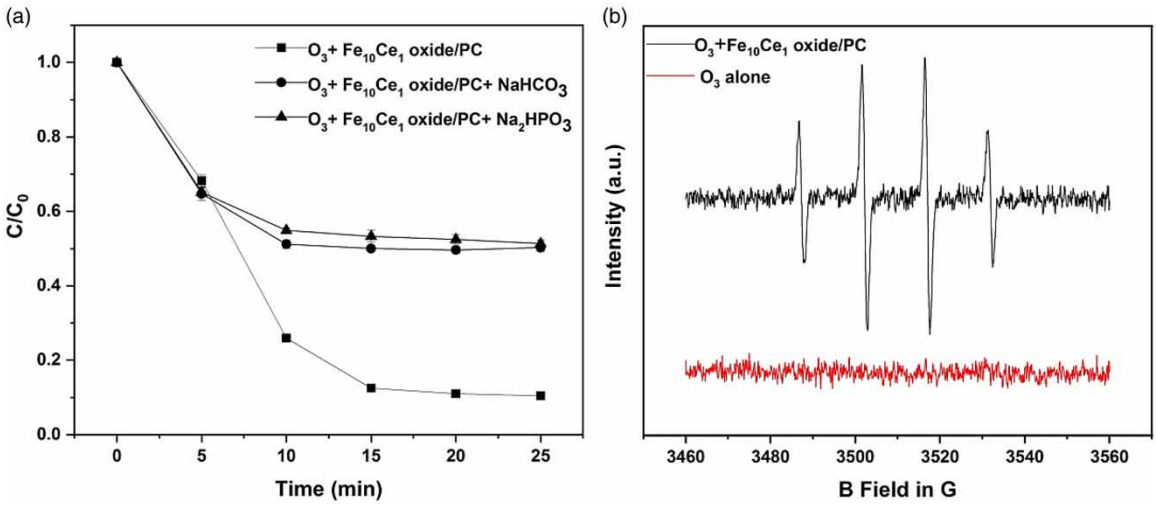

Figure 6 | (a) Influence of HCO_3^- and PO_4^{3-} on catalytic ozonation; (b) ESR spectra of DMPO-OH signal in the ozonation systems.

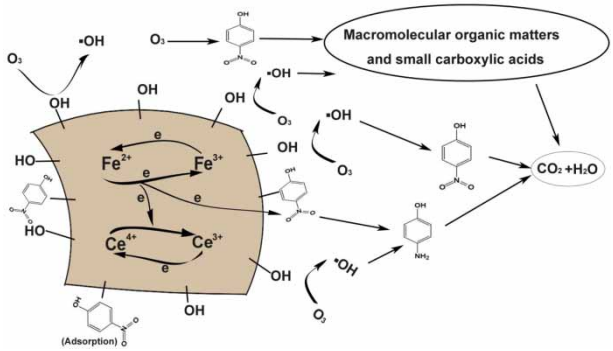

Figure 7 | The proposed reaction mechanisms of $Fe_{10}Ce_1$ oxide/PC.

Figure 7 shows the schematic diagram of the mechanism with $Fe_{10}Ce_1$ oxide/PC in catalytic ozonation. According to Figure 1(b), when ozone was added alone, the TOC of PNP had a removal rate of about 40%. The selectivity of the ozone molecule in oxidation showed that it could directly degrade PNP to macromolecular carboxylic acid substances. Due to its characteristics, ozone molecules could be connected with H and O of hydroxyl groups on the surface of the catalyst to produce •OH, which could be directly detected from the solution, has a higher Redox potential than the O_3 molecule, and could improve the degradation efficiency of PNP to 90% in the catalytic ozonation process (Wang & Bai 2017). The reason that the degradation efficiency of $Fe_{10}Ce_1$ oxide was low might be the adsorption of $Fe_{10}Ce_1$ oxide/PC could not only degrade a part of, but also led the catalyst to produce oxygen vacancy after adsorption on the catalyst surface, improving the electron transfer efficiency (Huang *et al.* 2016).

CONCLUSION

The magnetic catalyst $Fe_{10}Ce_1$ oxide/PC prepared by the pyrolysis of cotton textile wastes could thoroughly remove 90% PNP in the aqueous solution when the reaction time was 25 min. It is a green and recoverable catalyst with superior performance. The main composition of the material was analyzed according to a series of characterizations, and $Fe_{10}Ce_1$ oxide/PC had a high surface area and pores to absorb and degrade pollutants. Catalytic degradation follows the free radical mechanism. The adsorption property of the material itself and the introduction of metal ions increased the active sites for ozone adsorption. The electron transfer of Fe^{2+}/Fe^{3+} and Ce^{4+}/Ce^{3+} ions generated more hydroxyl radicals to degrade PNP completely. Through RSM experiments, the optimal experimental conditions were the initial pH of 9, the catalyst dosage of 0.4 g/L, and the ozone addition of 1.77 L/min (5.9 mg/L). Therefore, the synthesis of $Fe_{10}Ce_1$ oxide/PC using cotton textile waste material will have a good application prospect.

ACKNOWLEDGEMENTS

This work was supported by the National Natural Science Foundation of China (No. 21876111) and National Natural Science Foundation of China (No. 41772331).

DATA AVAILABILITY STATEMENT

All relevant data are included in the paper or its Supplementary Information.

REFERENCES

Afzal, S., Quan, X. & Lu, S. 2019 Catalytic performance and an insight into the mechanism of CeO_2 nanocrystals with different exposed facets in catalytic ozonation of p-nitrophenol. *Applied Catalysis B: Environmental* **248**, 526–537. doi:10.1016/j.apcatb.2019.02.010.

Asgari, G., Seidmohammadi, A., Esrafili, A., Faradmal, J., Noori Sepehr, M. & Jafarinia, M. 2020 The catalytic ozonation of diazinon using nano-MgO@CNT@Gr as a new heterogenous catalyst: the optimization of effective factors by response surface methodology. *RSC Advances* **10** (13), 7718–7731. doi:10.1039/c9ra10095d.

Bader, H. & Hoigné, J. 2013 Determination of ozone in water by the indigo method. *Water Research* **15** (4), 449–456.

Canizares, P., Lobato, J., Paz, R., Rodrigo, M. A. & Saez, C. 2005 Electrochemical oxidation of phenolic wastes with boron-doped diamond anodes. *Water Research* **39** (12), 2687–2703. doi:10.1016/j.watres.2005.04.042.

Chen, X., Murugananthan, M. & Zhang, Y. 2016 Degradation of p-Nitrophenol by thermally activated persulfate in soil system. *Chemical Engineering Journal* **283**, 1357–1365. doi:10.1016/j.cej.2015.08.107.

Chen, C., Han, Y., Guo, J., Zhou, L. & Lan, Y. 2018 Assessing the role of silica gel in the degradation of p-nitrophenol via Zn(0)-activated persulfate. *Journal of the Taiwan Institute of Chemical Engineers* **88**, 169–176. doi:10.1016/j.jtice.2018.03.053.

Dai, Q., Wang, J., Chen, J. & Chen, J. 2014 Ozonation catalyzed by cerium supported on activated carbon for the degradation of typical pharmaceutical wastewater. *Separation and Purification Technology* **127**, 112–120. doi:10.1016/j.seppur.2014.01.032.

Derakhshan, M. & Fazeli, M. 2018 Improved biodegradability of hardly-decomposable wastewaters from petrochemical

industry through photo-Fenton method and determination of optimum operational conditions by response surface methodology. *Journal of Biological Engineering* **12** (1). doi:10.1186/s13036-018-0104-9.

Fang, C., Gao, X., Zhang, X., Zhu, J., Sun, S. P., Wang, X., Wu, W. D. & Wu, Z. 2019 Facile synthesis of alkaline-earth metal manganites for the efficient degradation of phenolic compounds via catalytic ozonation and evaluation of the reaction mechanism. *Journal of Colloid and Interface Science* **551**, 164–176. doi:10.1016/j.jcis.2019.05.010.

Huang, Y., Long, B., Tang, M., Rui, Z., Balogun, M.-S., Tong, Y. & Ji, H. 2016 Bifunctional catalytic material: an ultrastable and high-performance surface defect CeO_2 nanosheets for formaldehyde thermal oxidation and photocatalytic oxidation. *Applied Catalysis B: Environmental* **181**, 779–787. doi:10.1016/j.apcatb.2015.08.047.

Huang, Y., Yang, T., Liang, M., Wang, Y., Xu, Z., Zhang, D. & Li, L. 2019 Ni-Fe layered double hydroxides catalized ozonation of synthetic wastewater containing Bisphenol A and municipal secondary effluent. *Chemosphere* **235**, 143–152. doi:10.1016/j.chemosphere.2019.06.162.

Li, Y.-X., Wang, X., Wang, C.-C., Fu, H., Liu, Y., Wang, P. & Zhao, C. 2020 S-TiO_2/UiO-66-NH_2 composite for boosted photocatalytic Cr(VI) reduction and bisphenol A degradation under LED visible light. *Journal of Hazardous Materials* **399**, 123085. doi:10.1016/j.jhazmat.2020.123085.

Li, S., Wu, Y., Zheng, Y., Jing, T., Tian, J., Zheng, H., Wang, N., Nan, J. & Ma, J. 2021 Free-radical and surface electron transfer dominated bisphenol A degradation in system of ozone and peroxydisulfate co-activated by $CoFe_2O_4$-biochar. *Applied Surface Science* **541**, 147887. doi:10.1016/j.apsusc.2020.147887.

Lv, A., Hu, C., Nie, Y. & Qu, J. 2010 Catalytic ozonation of toxic pollutants over magnetic cobalt and manganese co-doped γ-Fe2O3. *Applied Catalysis B: Environmental* **100** (1–2), 62–67. doi:10.1016/j.apcatb.2010.07.011.

Lv, A., Hu, C., Nie, Y. & Qu, J. 2012 Catalytic ozonation of toxic pollutants over magnetic cobalt-doped Fe3O4 suspensions. *Applied Catalysis B: Environmental* **117–118**, 246–252. doi:10.1016/j.apcatb.2012.01.020.

Malakootian, M., Shahamat, Y. D. & Mahdizadeh, H. 2020 Purification of diazinon pesticide by sequencing batch moving-bed biofilm reactor after ozonation/Mg-Al layered double hydroxides pre-treated effluent. *Separation and Purification Technology* **242**, 116754. doi:10.1016/j.seppur.2020.116754.

Ohmukai, Y., Hasegawa, I., Fujisawa, H., Okuma, O. & Mae, K. 2008 Production of an iron-loaded carbonaceous material through pyrolyzing biomass impregnated with $FeCl_2$. *Fuel* **87** (10–11), 2041–2049. doi:10.1016/j.fuel.2007.12.013.

Pang, Y. & Lei, H. 2016 Degradation of p-nitrophenol through microwave-assisted heterogeneous activation of peroxymonosulfate by manganese ferrite. *Chemical Engineering Journal* **287**, 585–592. doi:10.1016/j.cej.2015.11.076.

Qi, L., Tang, X., Wang, Z. & Peng, X. 2017 Pore characterization of different types of coal from coal and gas outburst disaster sites using low temperature nitrogen adsorption approach. *International Journal of Mining Science and Technology* **27** (2), 371–377.

Qi, R., Zhang, D., Zhou, Y., Gao, Y., Xiong, M., Deng, H. & Xu, Z. 2020 Effect of dispersant on the synthesis of cotton textile waste-based activated carbon by $FeCl_2$ activation: characterization and adsorption properties. *Environmental Science and Pollution Research International* doi:10.1007/s11356-020-10321-1.

Rodrigues, C. S. D., Borges, R. A. C., Lima, V. N. & Madeira, L. M. 2018 p-Nitrophenol degradation by Fenton's oxidation in a bubble column reactor. *Journal of Environment Management* **206**, 774–785. doi:10.1016/j.jenvman.2017.11.032.

Shen, Y., Xu, Q., Gao, D. & Shi, H. 2017 Degradation of an anthraquinone dye by Ozone/Fenton: response surface approach and degradation pathway. *Ozone: Science & Engineering* **39** (4), 219–232. doi:10.1080/01919512.2017.1301245.

Shen, T., Zhang, X., Lin, K. A. & Tong, S. 2020 Solid base Mg-doped ZnO for heterogeneous catalytic ozonation of isoniazid: performance and mechanism. *Science of the Total Environment* **703**, 134983. doi:10.1016/j.scitotenv.2019.134983.

Tian, D., Xu, Z., Zhang, D., Chen, W., Cai, J., Deng, H., Sun, Z. & Zhou, Y. 2019 Micro–mesoporous carbon from cotton waste activated by $FeCl_3$/$ZnCl_2$: preparation, optimization, characterization and adsorption of methylene blue and eriochrome black T. *Journal of Solid State Chemistry* **269**, 580–587. doi:10.1016/j.jssc.2018.10.035.

Wang, J. & Bai, Z. 2017 Fe-based catalysts for heterogeneous catalytic ozonation of emerging contaminants in water and wastewater. *Chemical Engineering Journal* **312**, 79–98. doi:10.1016/j.cej.2016.11.118.

Wang, J. & Chen, H. 2020 Catalytic ozonation for water and wastewater treatment: recent advances and perspective. *Science of the Total Environment* **704**, 135249. doi:10.1016/j.scitotenv.2019.135249.

Wang, T., Zhou, Y., Cao, S., Lu, J. & Zhou, Y. 2019 Degradation of sulfanilamide by Fenton-like reaction and optimization using response surface methodology. *Ecotoxicology and Environmental Safety* **172**, 334–340. doi:10.1016/j.ecoenv.2019.01.106.

Wu, Z.-w., Xu, X.-c., Jiang, H.-b., Zhang, R.-y., Song, S.-n., Zhao, C.-q. & Yang, F.-l. 2017 Evaluation and optimization of a pilot-scale catalytic ozonation–persulfate oxidation integrated process for the pretreatment of dry-spun acrylic fiber wastewater. *RSC Advances* **7** (70), 44059–44067. doi:10.1039/c7ra03287 k.

Xiao, Z., Huang, Y.-C., Dong, C.-L., Xie, C., Liu, Z., Du, S., Chen, W., Yan, D., Tao, L., Shu, Z., Zhang, G., Duan, H., Wang, Y., Zou, Y., Chen, R. & Wang, S. 2020 Operando identification of the dynamic behavior of oxygen vacancy-rich Co_3O_4 for oxygen evolution reaction. *Journal of the American Chemical Society* **142** (28), 12087–12095. doi:10.1021/jacs.0c00257.

Xu, Z., Zhang, T., Yuan, Z., Zhang, D., Sun, Z., Huang, Y., Chen, W., Tian, D., Deng, H. & Zhou, Y. 2018 Fabrication of cotton textile waste-based magnetic activated carbon using $FeCl_3$

activation by the Box–Behnken design: optimization and characteristics. *RSC Advances* **8** (66), 38081–38090. doi:10.1039/c8ra06253f.

Xu, Z., Gu, S., Sun, Z., Zhang, D., Zhou, Y., Gao, Y., Qi, R. & Chen, W. 2020 Synthesis of char-based adsorbents from cotton textile waste assisted by iron salts at low pyrolysis temperature for Cr(VI) removal. *Environmental Science and Pollution Research International* **27** (10), 11012–11025. doi:10.1007/s11356-019-07588-4.

Yu, S., Hu, J. & Wang, J. 2010 Gamma radiation-induced degradation of p-nitrophenol (PNP) in the presence of hydrogen peroxide (H_2O_2) in aqueous solution. *Journal of Hazardous Materials* **177** (1–3), 1061–1067. doi:10.1016/j.jhazmat.2010.01.028.

Yuan, L., Shen, J., Yan, P. & Chen, Z. 2018 Interface mechanisms of catalytic ozonation with amorphous iron silicate for removal of 4-Chloronitrobenzene in aqueous solution. *Environmental Science and Technology* **52** (3), 1429–1434. doi:10.1021/acs.est.7b04875.

Zhang, C., Li, B., Cai, M., Xiao, Q. & Shen, J. 2016 Nitrogen-doped activated carbon for a high energy hybrid supercapacitor. *Energy & Environmental Science: EES* **9** (1), 102–106.

Zhang, J., Xiong, Z., Wei, J., Song, Y., Ren, Y., Xu, D. & Lai, B. 2020 Catalytic ozonation of penicillin G using cerium-loaded natural zeolite (CZ): efficacy, mechanisms, pathways and toxicity assessment. *Chemical Engineering Journal* **383**, 123144. doi:10.1016/j.cej.2019.123144.

Zhao, H., Dong, Y., Wang, G., Jiang, P., Zhang, J., Wu, L. & Li, K. 2013 Novel magnetically separable nanomaterials for heterogeneous catalytic ozonation of phenol pollutant: $NiFe_2O_4$ and their performances. *Chemical Engineering Journal* **219**, 295–302. doi:10.1016/j.cej.2013.01.019.

First received 15 January 2021; accepted in revised form 23 March 2021. Available online 5 April 2021